Structure of the Toxic Domain of the *Escherichia coli* Heat-Stable Enterotoxin ST I†

Jean Gariépy,*,‡ Andrew Lane,§ Felix Frayman,§,∥ David Wilbur,§,⊥ Wolfgang Robien,§,# Gary K. Schoolnik,‡ and Oleg Jardetzky§

Department of Medical Microbiology, Stanford University, and Stanford University Magnetic Resonance Laboratory, Stanford, California 94305

Received May 9, 1986; Revised Manuscript Received July 21, 1986

ABSTRACT: Active fragments of the heat-stable enterotoxin ST I of *Escherichia coli* were chemically synthesized with the sequence Cys-Cys-Glu-Leu-Cys-Cys-Asn-Pro-Ala-Cys-Thr-Gly-Cys-(Tyr) and studied by proton (^{1}H NMR) and carbon-13 (^{13}C NMR) nuclear magnetic resonance spectroscopy as a function of pH and temperature. All of the nonexchangeable protons in the ^{1}H NMR spectrum were assigned. Although all amide protons were present at temperatures below 25 °C and pH values below 6, some of the resonances are broad and could not be assigned. The temperature dependence of these broad resonances indicates a change in conformation that is localized in the N-terminus. Other amide protons disappear at higher temperatures owing to chemical exchange with the solvent. Sufficient resonance assignments can be made at high and low temperatures to permit structural conclusions to be made. The chemical shifts of the α-carbon protons indicate the presence of substantial structure, which was further defined with the observed pattern of nuclear Overhauser enhancements (NOEs), coupling constants, and exchange rates. The NMR data identify a turn from Ala-14 to Cys-18. A second likely turn is centered around the proline residue. An interresidue NOE between the α-carbon protons of Asn-12 and Gly-17 indicates that the molecule folds back on itself. The NMR information is sufficient to define the structure of the C-terminal region of ST I. Manual model building then indicated that one arrangement of the three disulfides is particularly compatible with the NMR data and van der Waals constraints. A model incorporating the disulfide arrangement proposed by Houghten and his co-workers [Houghten, R. A., Ostresh, J. M., & Klipstein, F. A. (1984) *Eur. J. Biochem. 145*, 157–162] and the NMR constraints was derived with the programs PROTO [Frayman, F. (1985) Ph.D. Thesis, Northwestern University] and NOEMOT [Lane, A. N., Lefèvre, J.-F., & Jardetsky, O. (1986) *Biochim. Biophys. Acta 867*, 45–56].

Enterotoxigenic *Escherichia coli* strains elaborate three recognized classes of enterotoxins that cause secretory diarrheas in young children living in developing countries (Walsh & Warren, 1979; Sack, 1980). One of these toxins, abbreviated ST I, is an 18 or 19 amino acid peptide (So & McCarthy, 1980; Aimoto et al., 1982; Moseley et al., 1983; Thompson & Giannella, 1985). The mode of action of ST I is linked to its ability to activate particulate guanylate cyclase in the brush border membrane of intestinal epithelial cells (Field et al., 1978; Hughes et al., 1978; Giannella & Drake, 1979). We and others have reported the specific binding of radiolabeled ST I to rat enterocytes (Giannella et al., 1983; Frantz et al., 1984) and to rat intestinal membranes (Dreyfus & Robertson, 1984; Gariépy & Schoolnik, 1986; Kuno et al., 1986). Two or more proteins have been identified as parts of a putative ST I receptor on intestinal membranes (Gariépy & Schoolnik, 1986; Kuno et al., 1986). The enterotoxic and receptor-binding functions of ST I have been mapped to a C-terminal 13 amino acid segment, which includes six cysteines (Yoshimura et al., 1985; Gariépy & Schoolnik, 1986). Homologous sequences have now been reported for similar enterotoxins produced by some strains of *Yersinia enterocolitica* and *Vibrio cholerae* (Takao et al., 1984, 1985). A detailed knowledge of the structure of ST I in solution would complement biochemical and synthetic strategies aimed at defining the functional groups of ST I necessary for receptor recognition and diarrheal activity. To this end, we have chemically synthesized two active analogues, abbreviated ST Ib(6–18)[1] and ST Ib(6–19), for nuclear magnetic resonance (NMR) studies. The secretory activity in suckling mice and the receptor-binding function of these analogues are equipotent with those of native ST I (Gariépy & Schoolnik, 1986; Kuno et al., 1986). These analogues therefore contain all the structural information responsible for the toxin's functions. On the basis of NMR and van der Waals constraints as well as a suggested set of disulfide connectivities (Houghten et al., 1984), we propose a structure for these synthetic analogues.

† This investigation was supported by research grants from NIH (RR0771) and by research allowances from the Alberta Heritage Foundation for Medical Research (to J.G.). J.G. is a fellow of the Medical Research Council of Canada. G.K.S. is a fellow of the John Hartford Foundation.

* Address correspondence to this author at the Ontario Cancer Institute, Toronto, Ontario, Canada M4X 1K9.

‡ Stanford University.

§ Stanford University Magnetic Resonance Laboratory.

∥ Present address: Intelligent System Laboratory, Xerox Palo Alto Research Center, Palo Alto, CA 94304.

⊥ Present address: Varian Associates, Palo Alto, CA.

Present address: Institut fur Organische Chemie, Wien, Austria.

[1] Abbreviations: NMR, nuclear magnetic resonance; COSY, two-dimensional homonuclear shift-correlated spectroscopy; NOE, nuclear Overhauser enhancement; NOESY, two-dimensional nuclear Overhauser enhancement spectroscopy; ST Ib, a 19 amino acid long heat-stable enterotoxin purified from an enterotoxigenic *Escherichia coli* strain by Aimoto et al. (1982); ST Ib(6–18), synthetic analogue of ST Ib comprising residues 6–18; ST Ib(6–19), synthetic analogue of ST Ib comprising residues 6–19.

0006-2960/86/0425-7854$01.50/0

Experimental Procedures

Preparation of Synthetic Analogues. The peptides were prepared by solid-phase peptide synthesis on a Beckman 990B peptide synthesizer (Beckman Instruments, Inc., Fullerton, CA). The synthesis and purification of these analogues were performed as described elsewhere (Gariépy et al., 1984). Purified ST Ib(6–19) and ST Ib(6–18) cause diarrhea in suckling mice (<5 ng) and can compete as well as natural ST I for receptor sites on intestinal membranes (Gariépy et al., 1984; Gariépy & Schoolnik, 1986; Kuno et al., 1986).

Preparation of NMR Samples. The purified peptides were repeatedly lyophilized from D_2O to exchange the amide protons. The samples were finally dissolved in 600 μL of 99.8% D_2O, and the pH was adjusted to a pD of 6 with a 1 M NaOD solution. The pH meter reading was not corrected for isotope effects. The final peptide concentration was 7.4 mM for ST Ib(6–19) and 16.5 mM for the ST Ib(6–18) analogue. For the assignment of amide protons, the peptide samples were relyophilized and redissolved in 600 μL of 15% D_2O–85% H_2O. The sample pH was adjusted to 5. Carbon-13 NMR experiments were performed on a 4 mM sample of ST Ib(6–18) dissolved in D_2O in a 10-mm probe. Broad-band proton decoupling was employed during both acquisition and delays, with lower power during the latter to reduce heating effects.

NMR Experiments. Proton NMR spectra were recorded at 500 MHz on a JEOL GX-500 NMR spectrometer. Spectra were referenced to internal 2,2′-dimethylsilapentane-5-sulfonate (DSS). The spectra were assigned to spin type by homonuclear correlated (COSY) spectroscopy in D_2O (Bax, 1981; Nagayama, 1981). Sequential assignments were made with NOESY and COSY in H_2O (Billeter et al., 1982; Zuiderweg et al., 1984) at low temperatures (10 °C) to increase the tumbling time of the molecule. Further assignments were obtained from 2D *J*-resolved spectra at 10 °C.

The stability of the amide protons was assessed as follows. The chemical shift of the amide protons varies in a linear fashion as the temperature is increased, the slope of this dependence reflecting the strength of the hydrogen bond (Wüthrich, 1976). The intensity of the amide protons decreases as the temperature is raised if there is significant exchange with the solvent but increases if they do not exchange on the time scale of seconds. As the intrinsic rate of exchange is specifically base catalyzed (Wagner, 1984; Englander & Kallenbach, 1984), the lines become broader as the pH is raised, and the relative intensity decreases. The pH was varied by adding small aliquots of 1 M NaOH or 1 M HCl or 0.6 M sodium phosphate, pH 7.6, to the sample in the NMR tube, and the pH was measured with a microelectrode. Finally, the spin–lattice relaxation time (T_1) is also sensitive to exchange (Kearns, 1984). By combining the different pieces of information, it is possible to decide which protons exchange most rapidly under different conditions. The most rapidly exchanging protons can be identified as those not involved in hydrogen bonds.

Nonselective T_1 experiments were performed with the inversion recovery method (Gupta et al., 1982). Selective T_1 experiments were performed with a short pulse (25 ms) from the decoupler at a particular frequency, and a $\bar{1}3\bar{3}\bar{1}$ observation pulse as previously described (Hore, 1983; Lefèvre et al., 1985).

Model Building. Initial models were built to fit the NMR data and van der Waals constraints with CPK models. A Nicholson model was then constructed, from which approximate torsion angles were estimated. These angles were compared, where appropriate, with the values estimated from $^3J_{C^\alpha\text{–NH}}$.

A structure consistent with the experiment data was then derived with the program PROTO (Frayman, 1985) that incorporates van der Waals contact distances (Ramachandran, 1968) and distances derived from NOEs, as well as geometric constraints for disulfide bridges (Thornton, 1981; Richardson, 1981) and hydrogen bonds (Baker, 1984). The program is first seeded with the primary sequence of the peptide having its amino acids in conformations given by the Brookhaven Data Bank. A structure is derived by varying dihedral angles in the peptide sequence, which minimizes the error function associated with the input constraints. Multiple runs of the program are performed with the results of previous runs taken as input for the subsequent ones. The runs can be divided into the following groups, on the basis of the considered constraints and corresponding dihedral angles that affect these constraints:

First Group. (1) van der Waals constraints on the backbone (excluding the side chains); (2) distance constraints on sequential amino acids derived from NOEs.

Second Group. Same as the first group with the addition of (1) all distance constraints derived from NOEs; (2) distance constraints between C^β atoms of cysteine as imposed by their proximity in a disulfide linkage.

Third Group. Same as the second group with the addition of (1) van der Waals constraints on the cysteine side chains; (2) distance constraints between sulfur atoms of cysteine as imposed by the three disulfide bridges.

Fourth Group. Same as the third group with the addition of van der Waals constraints on all side chains.

Fifth Group. Same as the fourth group with the addition of negative hydrogen bonding information, where rapidly exchanging amide protons are not within 3 Å of any hydrogen bond acceptors.

Each run within these groups differs in the way the optimized error function is constructed. For unresolved diastereoscopic proton subsets, the distance constraints derived from NMR experiments were applied from a spatial position central to the protons in each subset. A complete description of the program is given by Frayman (1985).

The NOE data were also checked by an algorithm that simulates complete NOE time courses for an arbitrary number of spins (program NOEMOT; Lane et al., 1986a). In this algorithm, all interproton distances are calculated from the Cartesian coordinates in this instance generated by PROTO and translated into cross-relaxation rate constants (σ) and spin–lattice relaxation rate constants (ρ) according to (Kearns, 1984; Lane et al., 1986b)

$$\sigma = \alpha[6J(2\omega) - J(0)]/r^6 \tag{1}$$

$\rho =$

$$\alpha[J(0) + 3J(\omega) + 6J(2\omega)]\sum 1/r^6 \text{ over all pairs of protons} \tag{2}$$

where $\alpha = 0.1\gamma^4h^2(3/16\pi^2)$, γ is the gyromagnetic ratio and h is Planck's constant. $\alpha = 5.692 \times 10^{-38}$ cm^6 s^{-2}. $J(\omega)$ are the spectral density functions and are related to the correlation time τ by

$$J(\omega) = \tau/(1 + \omega^2\tau^2) \qquad J(0) = \tau \tag{3}$$

For equivalent protons (e.g., methyl groups), the term $J(0)$ in the expression for ρ drops out, and cross-correlation effects for rotating methyl groups were ignored. For amide protons, another term has to be added to ρ to account for dipole–quadrupole relaxation between the proton and the ^{14}N nucleus (Kearns, 1984). Once the appropriate relaxation rate constants have been calculated, the magnetizations of all spins are set to unity, except for the spin to be irradiated, whose magne-

Table I: Assignments of Proton Resonances for ST Ib Analogues at 20 °C[a]

assignment	NH	C^{α}	C^{β}	C^{γ}	C^{δ}
Glu-8	7.77/8.47	4.27	2.07	2.42, 2.72	
Leu-9	7.77/8.47	4.62	1.81, 1.69	1.52	0.93, 0.86
Asn-12	7.13	5.20	2.8, 2.73		
Pro-13		4.30	2.3	1.95	3.65
Ala-14	8.47	4.35	1.40		
Cys-15	7.71	4.60	3.48, 3.20		
Thr-16	8.57	4.05	4.07	1.27	
Gly-17	8.90	4.1, 3.75			
Cys-18	7.51	4.70	2.90		
Tyr-19	7.81	4.50	3.15, 2.90	6.85 (ring 2,6 H)	7.15 (ring 3,5 H)
unassigned cysteine spin systems					
Cys-7	(7.58)[b]				
Cys-10	6.92				
Cys-11	7.69				
		4.75	3.53, 3.18		
		4.50	3.13		
		4.37	3.25, 2.93		
		3.75	2.80		

[a] The amino acid sequence is listed in Figure 1. The assignments were made with a combination of COSY and NOESY spectra recorded in D_2O and in 85% H_2O–15% D_2O and pH titrations, as described in the text. Values in parentheses are tentative assignments. Chemical shifts for the analogue ST Ib(6–18) are within 0.08 ppm. [b] Determined from the pH titration of ST Ib(6–18).

tization is set to zero (high power limit; Bothner-By & Noggle, 1979). The magnetizations of the spins were calculated as a function of time by integrating the generalized Bloch equations:

$$\frac{dM_i}{dt} = -\rho_i(M_i - M_i^0) - \sum\sigma_{ij}(M_j - M_j^0) \qquad (4)$$

where M_i are the magnetizations and the superscript zero refers to the equilibrium value. The equations (4) were integrated by Euler's method, with the step size automatically adjusted to $^1/_{40}$ the fastest relaxing spin. The step size is halved at each iteration and the result compared with the original value. If the error is greater than 1%, the smaller step size is used. For slowly relaxing spins as in a small peptide, a step size of $1/(40\rho_{max})$ is adequate. The output consists of NOE buildup curves as a function of time for each proton in the system. The amplitudes of the NOE at any given time can then be compared with relative amplitudes observed experimentally. The method is described in more detail elsewhere (Lane et al., 1986a).

Internal motions were simulated by allowing atoms to move in a pseudoharmonic potential in three dimensions, subject to constraints of the covalent network and van der Waals radii (i.e., placing upper and lower bounds on internuclear distances). The amplitude and frequency of motion of each spin in each orthogonal direction was separately adjusted, and to avoid correlation of the motions, a random variation of the phase angle was allowed. Correlation times of each vector could also be varied.

The correlation time τ for the analogue ST Ib(6–19) was determined experimentally. The cross-relaxation rate constant for two spins having a fixed internuclear separation gives a measure of the effective correlation time, with no requirement that the shape or hydration be known (Olejnicjak et al., 1984; Lane et al., 1986b):

$$\sigma = \alpha[6J(2\omega) - J(0)]/r^6 \qquad (5)$$

where σ is the cross-relaxation rate constant and r is the internuclear separation. The spectral densities are related to the correlation time by eq 3. We chose the 2,6 and 3,5 protons of the tyrosine ring, whose distance r is 2.47 Å. Cross-relaxation rate constants were estimated from the initial slope of the NOE buildup curve, using the driven, truncated NOE (Wagner & Wüthrich, 1979). Since the tyrosine side chain may be independently mobile, this value yields a mimimum τ for the overall correlation of the compact molecule.

Results and Discussion

A detailed knowledge of ST I structure in solution is needed to delineate which functional groups of the enterotoxin are involved in peptide folding, receptor recognition, and diarrheal activity. The toxin's properties reside in a 13 amino acid segment that includes three intramolecular disulfide bridges, a feature leading to a highly constrained geometry. ST I is thus particularly suited to structural analysis by nuclear magnetic resonance spectroscopy. Two active analogues, termed ST Ib(6–18) and ST Ib(6–19), were synthesized and their NMR spectra analyzed with the initial goals of assigning proton resonances as well as tabulating geometric constraints. The constraints supplied by NOEs, coupling constants, and van der Waals radii in conjunction with a recently suggested disulfide arrangement (Houghten et al., 1984) were then used to propose a model for the peptide folding pattern.

(1) Resonance Assignments of ^1H NMR Spectrum. As shown in Figure 1, ST Ib(6–18) and ST Ib(6–19) differ by a single tyrosine residue at the C-terminus end of the molecule. For small peptides, spectral resonances can be efficiently assigned to particular protons by two-dimensional methods. Initially, general assignments to residue type are made with homonuclear correlated (COSY) spectroscopy in D_2O, a technique that manifests connectivities between J-coupled protons. All of the nonexchangeable protons were assigned to residue type and are listed in Table I. As eight of the amino acids are unique, they are automatically assigned to particular residues.

Sequential resonance assignments to particular amino acid residues were made by the method developed by Wuthrich and his co-workers (Billeter et al., 1982; Zuiderweg et al., 1984), where a combination of COSY and NOESY spectra of the peptides is recorded in H_2O solutions. The COSY spectrum displays through-bond connectivities between each peptide backbone NH and its adjacent α-carbon proton, while through-space connectivities in the NOESY spectrum are observed for amide protons in spatial proximity to protons from neighboring residues. Figure 2 shows a COSY spectrum of ST Ib(6–19) in 85% H_2O/15% D_2O. There are only eight cross peaks connecting the NH region to the $C^{\alpha}H$ region, indicating that at most eight residues can be completely assigned from such spectra. The sequential assignment proce-

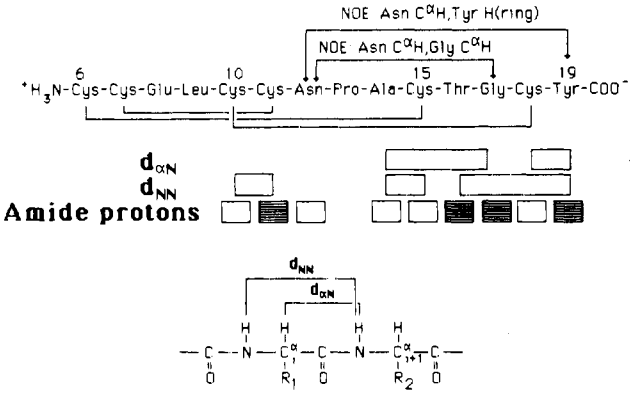

FIGURE 1: Amino acid sequence of ST Ib(6–19) and a summary of data derived from NMR experiments. In the rows $d_{\alpha N}$ and d_{NN}, boxes between two residues indicate that the proton distances $d_{\alpha N}$ or d_{NN} are less than 4 Å. These distances are defined in the diagram of a peptide segment. The open boxes in the last row (amide protons) indicate which amide protons are exchanging rapidly while the striped boxes represent relatively stable amide protons. The two long-range NOEs listed above the peptide sequence indicate the spacial proximity (<4 Å) of nonadjacent protons. A proposed set of disulfide bridges is indicated below the primary sequence of ST Ib(6–19) and was used as a constraint in our model building strategy.

dure was initiated with the amide proton triplet of Gly-17 located at the extreme low-field end of the spectrum (8.90 ppm). Glycine is the only residue that does not give doublets for its amide proton resonances. The two cross peaks in the COSY spectrum arise from *J*-coupling between the Gly-17 amide proton and its diastereotopic $C^{\alpha}H$ protons, reducing the number of useful peaks by one. Seven complete spin systems can be assigned, in addition to Pro-13, which has no amide proton. The amide proton assignments were confirmed by recording a NOESY spectrum of ST Ib(6–19) in H_2O (Figure 3). Although this spectrum was recorded at 10 °C to slow down exchange, and to increase the correlation time of the peptide, relatively few cross peaks are present. This is attributable to two effects: (1) competition between cross relaxation and chemical exchange with the solvent and (2) the presence of multiple conformations at low temperatures (see below). Nevertheless, by use of the combination of $d_{\alpha N}$ and d_{NN} connectivities (Figure 1), 9 of the 12 amide protons of ST Ib(6–19) were identified. The amide resonances of Cys-7, Glu-8, and Leu-9 remain to be assigned by other methods.

Figure 4 show a pH difference spectrum at 25 °C of the amide region of ST Ib(6–18), where Cys-18 now has a free carboxyl terminus. Removing Tyr-19 has no major effects on the chemical shifts of the amide protons (change in chemical shift <0.05 ppm), except for the removal of one, therefore confirming the assignment of the Tyr-19 amide proton. This also suggests that Tyr-19 plays no major structural role, in agreement with the observation that the 13 amino acid analogue ST Ib(6–18) retains all the functional properties of the native enterotoxin (Yoshimura et al., 1985; Gariépy & Schoolnik, 1986). The relative areas, obtained by approximating the peaks as triangles, are consistent with the presence of 11 protons at pH 2.8. Seven of these peaks are sharp (line widths <10 Hz), and four are relatively broad (>30 Hz). Hence, all of the expected protons are present under these conditions. The width of the four broad resonances could be due to exchange with the solvent or to the presence of more than one structure. Increasing the pH would be expected to broaden these resonances further if exchange with the solvent was important. For example, the positive peak at 8.97 ppm in the difference spectrum is due to the amide proton of Gly-17, which at pH 7.0 has a low intensity owing to exchange. However, the negative difference peak centered at 7.85 (Glu-8/Leu-9; Figure 4A) shows a significant change in chemical shift (this peak is positioned under the broad singlet at 7.7 ppm in the spectrum recorded at pH 2.8) without a large change in intensity, arguing against chemical exchange with the solvent.

The chemical shifts of the resonances in the spectrum of ST Ib(6–18) were similar to those of ST Ib(6–19). These assignments were confirmed in some cases, by an independent COSY experiment of the ST Ib(6–18) sample. Six of the amide proton resonances (assigned to Cys-10, Ala-14, Cys-15, Thr-16, Gly-17, and an unassigned resonance) shift less than 20 Hz downfield on changing the pH from 2.8 to 7.0. The resonance of Asn-12 moves 25 Hz downfield, whereas that of Cys-18 moves 115 Hz downfield. This large shift can be readily understood in terms of deprotonation of the free carboxy terminus of Cys-18, whose pK_a value is expected to be less than 3. The other small shifts can be ascribed to long-range perturbations by the ionization of the carboxy terminus. Two other resonances, which must arise from Cys-7, Glu-8, or Leu-9, shift 50 Hz upfield on raising the pH from 3.85 to 7.0. In fact, the chemical shift of these resonances changes more between pH 4 and pH 7 than between pH 2.8 and pH 4, in contrast to the resonance of Cys-18, where the change is greater at the lower pH range. The pK_a of the glutamic acid side chain is expected to lie above 4, suggesting that one of the upfield shifting peaks arises from Glu-8. Examination of a peptide model shows that the carboxyl side chain of Glu-8 can approach closely the amide protons of both Glu-8 and Leu-9 by simple rotation about the C^{α}–C^{β} bond but cannot readily approach the amide proton of Cys-7. Hence, we tentatively assign the resonances at 7.85 and 8.44 in the difference spectrum of Glu-8 and Leu-9. By elimination, the peak at 7.58 must belong to Cys-7. This resonance is essentially independent of pH. We can therefore use the chemical shift correspondences to assign the amide peaks of ST Ib(6–19) (Tables I and II).

(*2*) *Properties of Assigned Amide Resonances.* To determine the properties of the NH protons, we recorded ^1H NMR spectra as a function of temperature and pH.

(*a*) *Effect of Temperature on Amide Protons Reveals That Four Amide Protons Are Rapidly Exchanging.* Figure 5 shows the effect of temperature on the amide protons of ST Ib(6–19), at pH 6. At low temperatures, all of the amide protons are present, either as well-defined unique resonances, as overlapping peaks (i.e., Glu-8/Leu-9 and Ala-14 NH protons; 8.55 ppm region at 2 °C), or as broad multiplets (i.e., Cys-7/Glu-8/Leu-9 NH protons; 7.9 ppm region at 2 °C). As the temperature is raised above 20 °C, the triplet centered at 8.9 ppm (assigned to Gly-17 NH; Table I) and the Thr-16 amide proton resonance (8.57 ppm) decrease greatly in intensity, suggesting that these amide protons are labile, in agreement with the effect of pH on these resonances (section 2c).

The exchange properties of the amide protons can be studied by measuring their relative intensities as a function of temperature. If the temperature and viscosity affect line widths and intensities in approximately the same way for all protons, then the ratio of the intensities will be identical for all protons. If the ratio decreases as the temperature is raised, then it is likely that the NH resonances broaden with increasing temperature, due to exchange. We have chosen the resonance at 6.80 ppm as the reference line, which belongs to the nonexchangeable 2,6 protons of Tyr-19. The ratios of the intensities are given in Table III. Similarly, peaks assigned to the amide

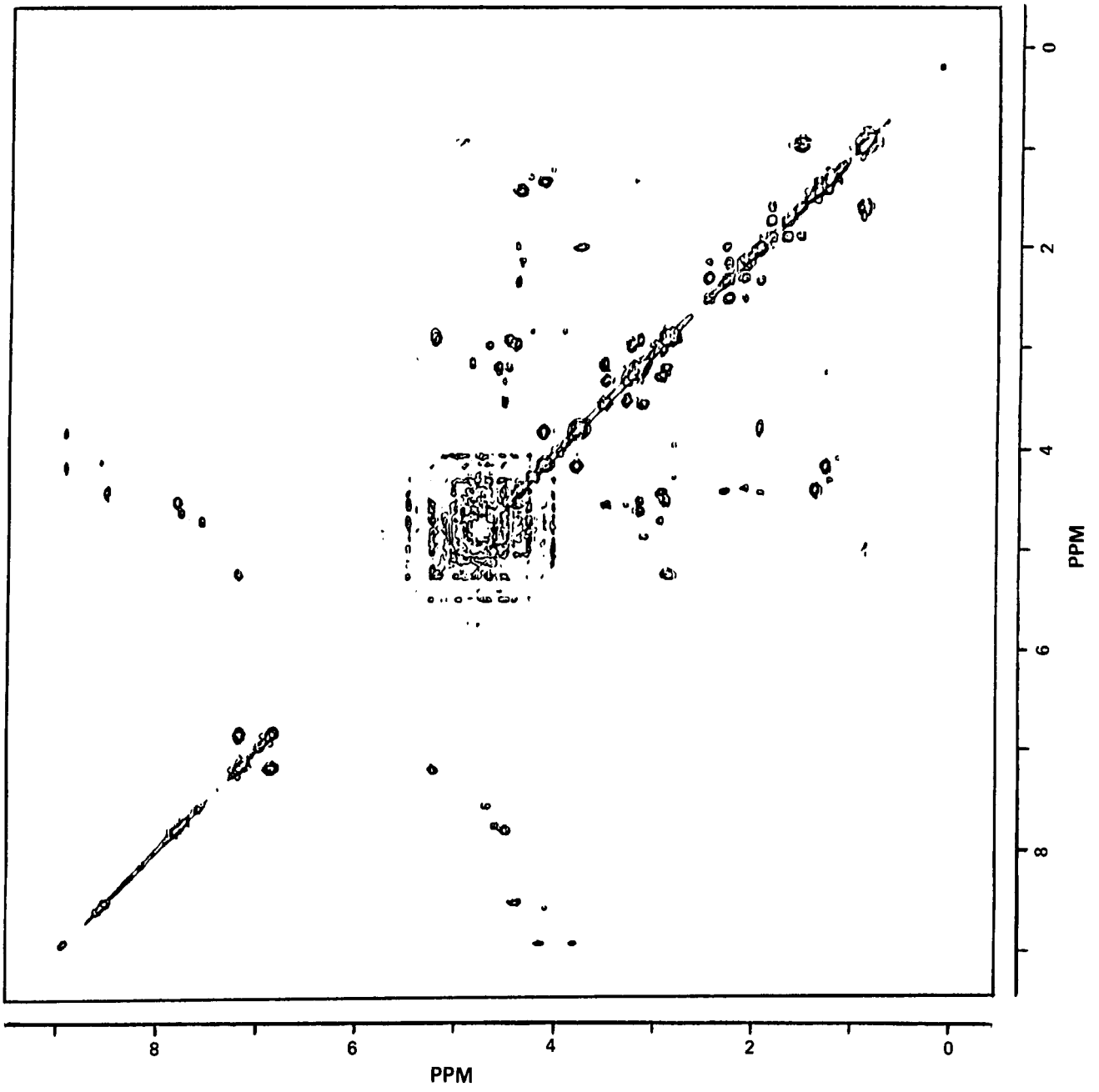

FIGURE 2: Contour plot of the region 0–9.4 ppm of the ^{1}H COSY spectrum at 500 MHz of ST Ib(6–19) in 15% D_2O–85% H_2O. The peptide concentration was 7.4 mM, pH 5, 10 °C. The spectrum was recorded with 1024 points in F_2 and 256, zero-filled to 512 points in F_1 over a spectral width of 5000 Hz. The FIDs were multiplied by an exponential (2 Hz line broadening) and a trapezoidal function set to 0, 20, 40, and 98% of the acquisition time in both dimensions. The spectrum was symmetrized and is displayed in the magnitude mode.

Table II: Properties of Amide Protons of ST Ib Analogues at 20 °C

assignment	chemical shift, δ (ppm)	line width (Hz)	T_1 (s)[a]	$d\delta/dT$ ($\times 10^3$ ppm/°C)	J (Hz)	dihedral angle, ϕ (deg)
Glu-8/Leu-9	(7.77)[b]	≈40	<0.4	≈0		
Glu-8/Leu-9	(8.47)	4[c]	0.68[c]	−1.1	7[c]	
Cys-10	6.92	<5	0.45	−3.7	3	
Cys-11	7.72	8[d]	<0.4	−5.2		
Asn-12	7.13	3	0.80	−1.7	8.5	60, −90, −150
Ala-14	8.47	4[c]	0.68[c]	−2.5	7[c]	25, 95, −85, −150
Cys-15	7.71	4[d]	0.68	−1.8	3.5[d]	
Thr-16	8.57	5	0.60	−5.6	4	
Gly-17	8.90	5	0.60	−6.4	≈7	
Cys-18	7.51	2.5	0.83	−1.4	9	60, −100, −140
Tyr-19	7.81	5	0.68	−6.5	8.5	60, −90, −150

[a] The data refer to a temperature of 2 °C. [b] Values in parentheses are tentative assignments. [c] The data refer to a temperature of 30 °C. [d] Overlapping resonances. T_1 is the nonselective spin–lattice relaxation time, J is the coupling constant, the line width was determined at half-height, and ϕ is the torsion angle (±30°) for the C^α–N bond derived from the coupling constant as described in section 2d.

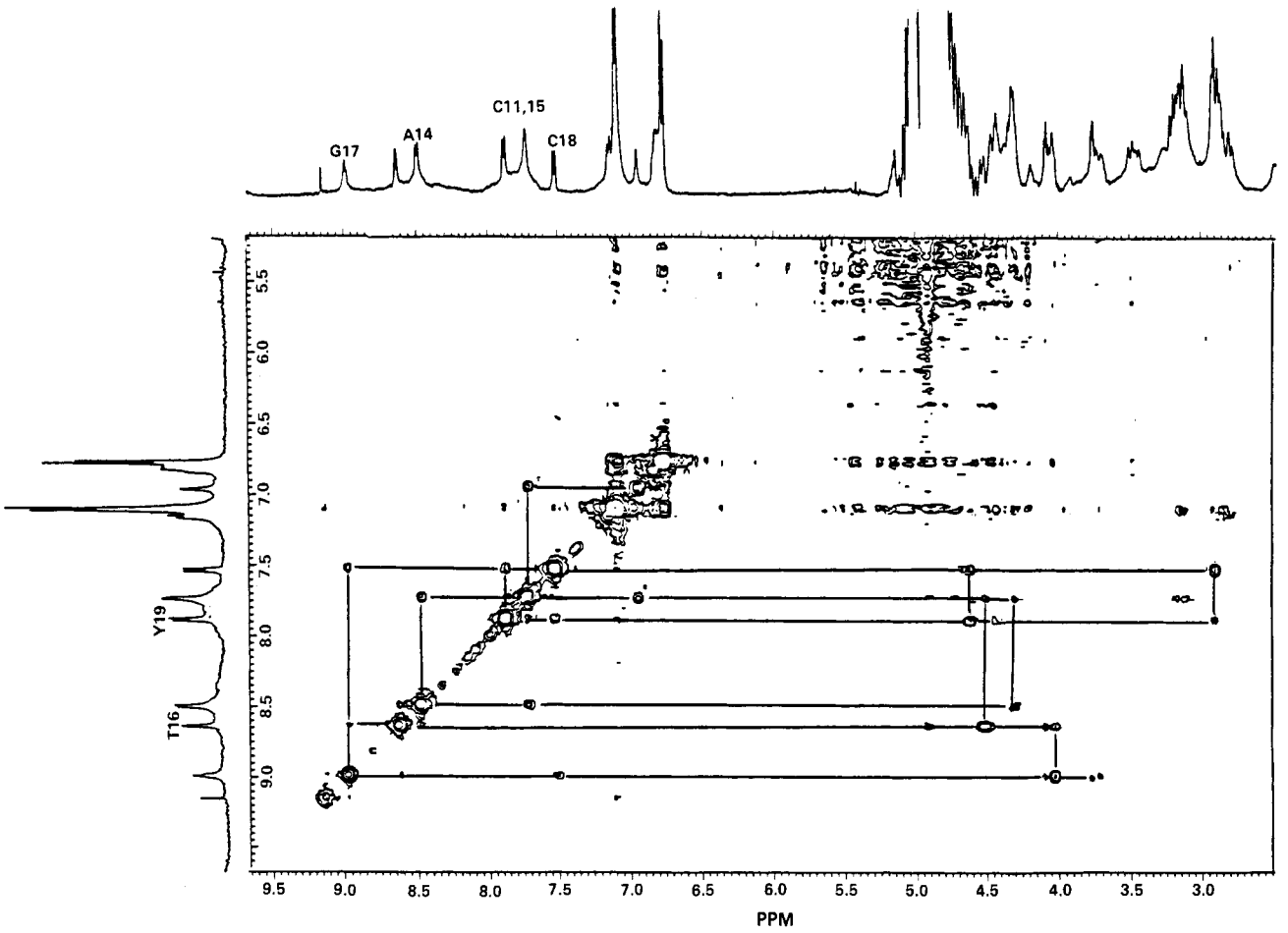

FIGURE 3: Contour plot of the spectral region F_1 = 2.5–9.6 ppm and F_2 = 5.2–9.6 ppm of the ^{1}H NOESY spectrum at 500 MHz of ST Ib(6–19) in 15% D_2O–85% H_2O. The peptide concentration was 7.4 mM, pH 5, 10 °C. The spectrum was recorded with 1024 points in F_2 and 256, zero-filled to 512 points in F_1 over a spectral width of 5000 Hz. The mixing time was 350 ms. Connectivities between amide and α-carbon protons (solid lines) can be used to trace part of the peptide backbone chain starting at Gly-17 NH (8.9 ppm).

Table III: Dependence of Relative Peak Heights of Amide Protons on Temperature[a]

	peak height ratio								
T (°C)	X	Cys-11	Asn-12	Ala-14	Cys-15	Thr-16	Gly-17	Cys-18	Tyr-19
2		0.13	0.13	0.23	0.19	0.21	0.21	0.23	0.24
10		0.14	0.21	0.22		0.19	0.16	0.23	0.24
20		0.13	0.19	0.24	0.20	0.14	0.13	0.23	0.24
30	0.08	0.13	0.21	0.24	0.20	0.12	0.10	0.24	0.24
40	0.14	0.14	0.24	0.24	0.21	0.10	0.06	0.26	0.22
50	0.17	0.11		0.20	0.21		0.035	0.22	0.20

[a] Peak heights were normalized to that of the tyrosine doublet at 6.85 ppm. pH = 6. X is the peak that becomes resolved at temperatures above 30 °C and assigned to Glu-8 or Leu-9 (Figure 5 and section 2a).

protons of Cys-11, Thr-16, and Gly-17, respectively, show evidence of significant exchange at this pH. On the other hand, peaks assigned to Asn-12, Ala-14, Cys-15, and Cys-18 show little evidence of exchange.

(*b*) *Detection of a Conformational Change.* Resonance line widths for amide protons are expected to broaden as proton exchange occurs. We observe a temperature-dependent sharpening and splitting of the broad resonance envelope positioned around 7.8 ppm (Cys-7 and Leu-9/Glu 8 NH protons, 2 °C). In addition, the weakly resolved peak centered at 7.75 ppm (Cys-11 and Cys-15 NH protons, 2 °C) splits into two doublets (7.77 and 7.67 ppm at 50 °C) and a broad singlet (7.54 ppm at 50 °C). These results cannot be ascribed solely to exchange with the solvent but rather to a change in conformation of the molecule. Indeed, the relative intensity of the doublet that appears near 7.8 ppm as the temperature is raised increases faster than those of other slowly exchanging amide protons (Figure 5; Table III), and its chemical shift is almost independent of the temperature in the range 30–50 °C. Note that at 50 °C, the amide proton doublet of Glu-8 (8.44 ppm) is resolved from the NH doublet of Ala-14 (8.39 ppm), while the Thr-17 NH resonance broadens and vanishes (Figure 5).

The dependence of the chemical shift of amide protons on temperature gives useful information about their relative stabilities. A large temperature coefficient ($d\delta/dT$ values, Table II) is consistent with rapid exchange and the absence of strong hydrogen bonding. The temperature coefficients are greatest for Cys-11, Thr-16, Gly-17, and Tyr-19 ($\geq$–5.2 ppb/°C) and smallest for the resonances of Glu-8, Asn-12, Ala-14, Cys-15, and Cys-18 ($\leq$–2.5 ppb/°C). The values of spin-relaxation time constants (T_1) are also indicators of the relative stability of the amide protons, with broad lines and short T_1 values pointing out a rapid exchange rate or con-

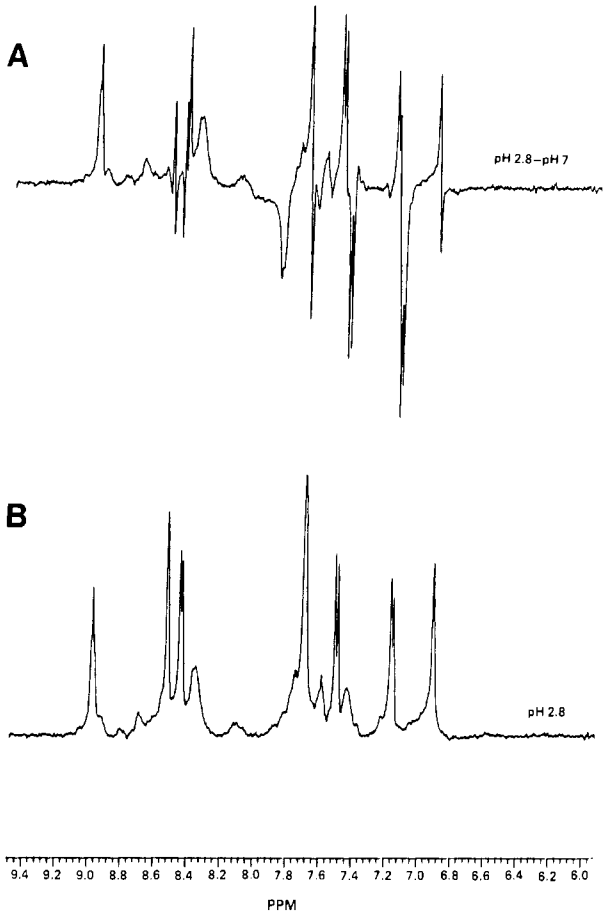

FIGURE 4: pH difference spectrum of the region 5.90–9.50 ppm of ST Ib(6–18) in 15% D_2O–85% H_2O. The peptide concentration was 16.5 mM, 25 °C. Spectra (512 accumulations) were recorded with 16 384 points over a spectral width of 5000 Hz. The FIDs were multiplied by a 2-Hz line-broadening exponential and subtracted after Fourier transformation and phasing. The solvent resonance was suppressed with the decoupler during the pulse delays (2 s). (A) Difference spectrum resulting from the subtraction of the ^1H NMR spectra recorded at pH 2.8 and 7. (B) Proton spectrum of ST Ib(6–18) recorded at pH 2.8.

formational flexibility. It is generally observed that those resonances having the largest temperature coefficients for their chemical shifts also have the broadest lines and the shortest T_1 values (Table II).

Another test for motion or conformational changes is the dependence of relaxation rates on temperature. For a rigid body, the relaxation rate constants should obey an Eyring relationship (Lane et al., 1986b):

$$\rho(T) = (A/T)\exp(E/RT) \quad (6)$$

where ρ is a relaxation rate constant, T is the absolute temperature, A is a constant, and E is the apparent activation energy for the viscosity of water (4 kcal/mol). Alternatively, the relaxation constants should follow the Perrin Law:

$$\rho(T) = B\eta/T \quad (7)$$

where B is another constant and η is the viscosity. Hence, plots of ln (ρT) vs. $1/T$ or ρ vs. η/T will be linear for rigid bodies. In the presence of internal motions, conformational changes, or chemical exchange, the Perrin plot may become nonlinear, and the Eyring plot may be either nonlinear or give an apparent activation energy substantially less than 4 kcal/mol. The apparent activation energy for a conformational change can be either greater or smaller than 4 kcal/mol (Lane et al., 1986b). The line widths for Asn-12, Ala-14, and Cys-18 all

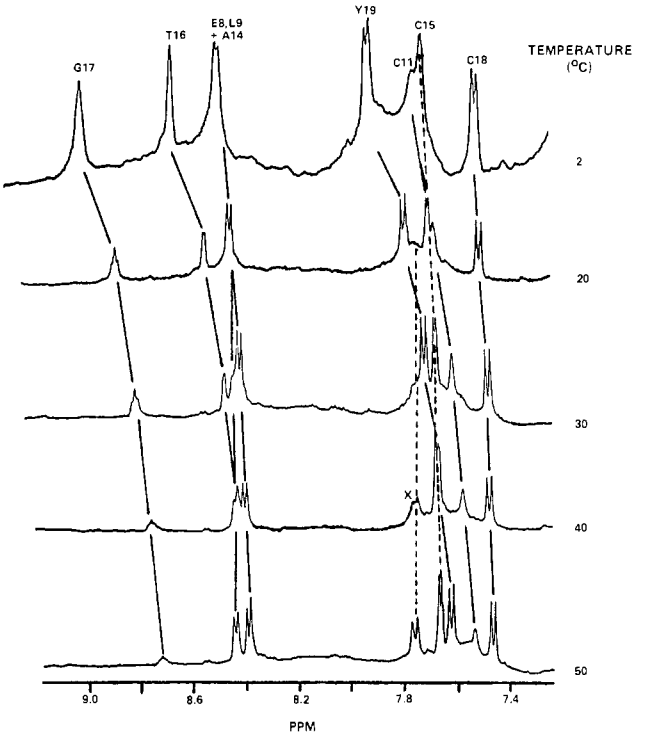

FIGURE 5: Effect of temperature on amide resonances of ST Ib(6–19). The peptide concentration was 7.4 mM, pH 6. Spectra were recorded with 16 384 points over a spectra width of 5000 Hz. The solvent resonance was suppressed with the decoupler during the pulse delays (2 s). Only the region 7.2–9.2 ppm is shown.

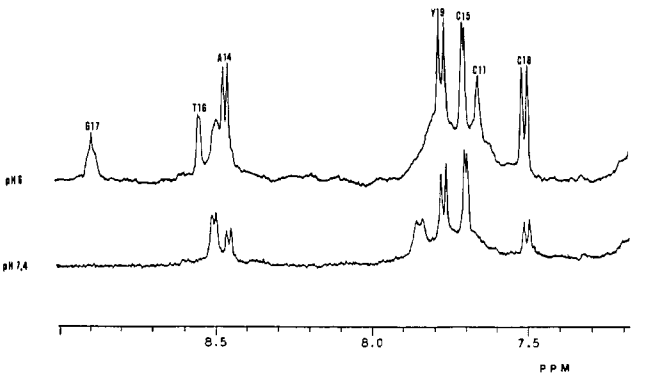

FIGURE 6: Effect on pH on amide resonances of ST Ib(6–19). The peptide concentration was 7.4 mM, 25 °C. Spectra (256 accumulations) were recorded with 16 384 points over a spectral width of 5000 Hz. (Upper trace) pH 6.0, in the absence of phosphate buffer; (lower trace) pH 7.4, in the presence of 40 mM phosphate buffer.

show linear Perrin and Eyring plots and given apparent activation energies of 4 kcal/mol, consistent with the absence of significant internal motions or conformational changes.

(*c*) *Dependence of Amide Proton Intensity on pH Identifies the Least Stable Protons.* The exchange of amide protons is base-catalyzed, and the rate is therefore dependent on the pH (Englander & Kallenbach, 1984). At pH 6, in the absence of buffer, all of the expected amide protons are visible in the spectrum of ST Ib(6–19) (Figure 6). On adding aliquots of 0.6 M phosphate to produce a final pH value of 7.4, the resonances assigned to Cys-11, Thr-16, and Gly-17 are broadened beyond detection. These protons exchange at essentially the intrinsic rate and are probably not hydrogen bonded. According to the data of Molday et al. (1972), the intrinsic rate constant for exchange should increase about 30-fold in this pH range. The intrinsic rate constant varies by a factor of about 3 along the sequence, with the exception

of Tyr-19, which is retarded owing to the end effect of the free carboxy terminus. Hence, the other protons presumably exchange more slowly than the intrinsic rate.

On the basis of temperature dependence of the amide proton chemical shifts ($d\delta/dT$), line widths, and intensities, as well as the effect of pH on resonance intensities and T_1 values (Figure 1; Tables II and III), we conclude the following: (1) The amide protons of Cys-11, Thr-16, Gly-17, and Tyr-19 are not hydrogen bonded. (2) The C-terminus from Asn-12 to Cys-18 forms a relatively well-ordered conformation independent of temperature. (3) The N-terminus from Cys-7 to Leu-9 or Cys-10 can exist in more than one conformational state depending on the temperature. Possibly only one is populated at high temperature (>40 °C), but at low temperatures at least two exist. (4) Asn-12, Ala-14, Cys-15, and Cys-18 amide protons are relatively stable and may be involved in hydrogen bonds.

(*d*) *Coupling Constants for NH to C$^{\alpha}$H Reveal That Several Backbone Dihedral Angles Are Conformationally Restricted.* The three-bond coupling constants ($^3J_{NHC^{\alpha}H}$) provide information about the range of C$^{\alpha}$–N dihedral angle (ϕ) accessible to conformationally restricted residues. The coupling constants are measured either from resolution-enhanced spectra or from 2D *J*-resolved spectra, using the tyrosine doublets at 7.14 and 6.85 ppm for calibration (J = 7.5 Hz). Only those coupling constants that are larger than 7–8 Hz can be used to comment on preferred angles, as smaller values could result from conformational averaging. However, several amide protons do have large coupling constants (Table II), implying that at least part of the molecule has a reasonably well-defined conformation in solution. The values of ϕ were estimated from the Karplus equation with the data of Ramachandran (1972), Bystrov (1976), De Marco et al. (1978), and Cung et al. (1981). The resolved coupling constants that have large values of J are associated with proton connectivities of residues located in the C-terminal part of the molecule, implying that the backbone of this region is conformationally restricted.

(*3*) *Carbon-13 Spectrum of ST Ib(6–18) Indicates Involvement of All Cysteines in Disulfide Bridges as well as the Presence of Cis–Trans Isomers of Pro-13.* The presence of disulfide linkages can be expected to limit the number of possible conformations accessible to the peptide. The lack of reactivity of ST I toward *N*-ethylmaleimide suggests that all six cysteines exist as cystine (Booth et al., 1984). The broad band decoupled ^{13}C NMR spectrum is in agreement with this result, as there are no signals in the 25 and 50–55 ppm regions that could be ascribed to cysteine (Wüthrich, 1976), whereas in the region 35–40 ppm there are too many signals present if there were no disulfide bridges. This conclusion is further confirmed by fast atom bombardment mass spectrometry, as the molecular ion is consistent only with a molecule in which all cysteines exist in disulfide bonds.

The carbon 13 NMR spectrum of ST Ib(6–18) suggests that Pro-13 exists in a cis–trans mixture, with approximately 60% of the cis isomer at 20 °C (~50% cis at 50 °C). There is no evidence of multiple resonances in the proton spectrum, implying that the effect of the isomerization may be local. The cis–trans conversion occurs along the dihedral angle ω_{Asn-12} (C'_{Asn-12} to N_{Pro-13} bond). Proline-13 may represent a molecular hinge between an amino-terminal region that exhibits averaged resonance signals on the NMR time scale (Cys-6 to Asn-12) and a structurally rigid C-terminal segment (Ala-14 to Tyr-19). In the case of insectotoxin I_5 A, a 35 amino acid peptide with four disulfide bridges, all three prolines occur in a trans configuration (Arseniev et al., 1984) giving rise to distinctive NOE cross-peaks for the $C^{\alpha}_{Pro-1}H$ and the $C^{\delta}_{Pro}H_2$ protons. We do not observe any NOE connectivities between $C^{\alpha}_{Asn}H$ and either $C^{\delta}_{Pro}H_2$ or $C^{\alpha}_{Pro}H$ protons. Conformational heterogeneity has been associated with the cis–trans isomerization of Pro-41 in the cardiac stimulants AP-A and ATX-II, two analogous peptides structurally constrained by multiple disulfide bridges (Gooley et al., 1984a,b; Gooley & Norton, (1985). Similarly, conotoxin MI, a small sea snail neurotoxin adopts two conformational states in solution (Gray et al., 1983). Since conotoxin MI and ST I have a similar sequence around their proline residue, it may well be that small differences in the energy barrier between cis and trans isomers of proline is responsible for observing these different conformations as discrete NMR resonances or as averaged signals.

(*4*) *Estimates of Rotational Correlation Time for Ring Protons of Tyr-19 Suggest That ST Ib(6–19) Is Not Spherical in Shape.* Measurements of the cross-relaxation rate constant for spin separated by a fixed distance give an estimate of the correlation time. We have measured the NOE build-up rate for the 3,5 and 2,6 phenolic ring protons of Tyr-19 at 5 and 25 °C. As the internuclear distance is fixed at 2.47 Å in the aromatic ring, we obtain estimates of the correlation time of 1.9 and 1.4 ns, respectively (eq 4). We have also measured the intrinsic spin–lattice relaxation rate constants for the ring and C$^{\beta}$ protons of Tyr-19 at 25 °C. The values are 0.75 and 3.23 s^{-1}, respectively. The distance between the diastereotopic C$^{\beta}$ protons is 1.8 Å and therefore dominates the relaxation of these protons. Adding the contribution from the C$^{\alpha}$ and 2,6 aromatic ring protons, we can estimate a lower limit of the correlation time of 1.3 ns at 25 °C. A similar calculation for the ring protons yields a lower limit of 1.4 ns at 25 °C. Hence, three independent measurements give similar values for the rotational correlation time. These values represent lower limits for the overall tumbling time since internal motion can only decrease the correlation time.

The molecular weight of ST Ib(6–19) is 1480, and its calculated partial specific volume is 0.69 (Zamyatnin, 1984). This leads to correlation times for rigid unhydrated spheres in D_2O of 1.0 and 0.54 ns at 5 and 25 °C. Three possibilities arise to explain the discrepancy. The molecule may aggregate into dimers at the concentration (7.4 mM) used in the experiments. However, the NMR spectra recorded at 7.4 and at 0.6 mM are identical in terms of chemical shifts are apparent line widths. In addition, the spin–lattice relaxation times of the resolved resonances (Tyr-19 ring protons, Asn-12 α-carbon proton, and the methyl resonances of Leu-8, Thr-16, and Ala-14) were independent of the concentration of the peptide within experimental error (±10%). An association into dimers would therefore have to be specific, with a dissociation constant much smaller than 0.6 mM. A second possibility for the high value of the measured correlation time is that the molecule is not spherical. For example, an ellipsoid having an axial ratio of 3:1 would have an effective correlation time about 30% higher than the equivalent sphere. A third possibility is that the molecule is hydrated, increasing its effective volume. Typical degrees of hydration of proteins range from 0.3 to 0.6 of water/g of protein (Cantor & Schimmel, 1981). The correlation times at 5 and 25 °C can be accounted for by an axial ratio of 3:1 and a degree of hydration of 0.6 of water/g of protein. Others combinations of number could account for the data, but given that the peptide must be compact, having three disulfide bonds, an axial ratio much greater that 3:1 is unlikely. A spherical shape would require the degree of hydration to be more than 1.1 g of water/g of

protein, which is unlikely. This suggests that the peptide has an elongated shape in solution.

The presence of significant internal motions can have large effects on NMR parameters, so that it is necessary to estimate the importance of internal motions on those parameters used for structural analysis. One important parameter is the $^3J_{NHC^\alpha H}$, which yields an estimate of the torsion angle ϕ. As the coupling constant typically varies from 0 to 10 Hz, motions occurring at rates larger than 100 s^{-1} are fast enough to average coupling constants. However, the Karplus equation indicates that if large coupling constants are observed ($J >$ 7–8 Hz), then averaging by rotations in the peptide backbone must be insignificant. The coupling constants for Asn-12, Ala-14, Cys-18, and Tyr-19 are all larger than 7 Hz (Table II) and are also independent of temperature in the range of 2–50 °C (Figure 5). This implies that there are no large amplitude excursions in the backbone of the C-terminal region in the time scale of 10 ns or shorter and also suggests that there are no significant changes in conformation of the backbone in this range of temperature.

(*5*) *Structural Conclusions from NMR Data.* From the data in Tables II and III, it is possible to decide which amide protons are not hydrogen bonded and to set boundary values for the torsion angle ϕ of particular residues in the peptide sequence. Other useful structural information is obtained from the NOESY spectrum in H_2O, in terms of connectivities between $C^\alpha H_i$ and NH_{i+1} protons ($d_{\alpha N}$ distance) and NH_i and NH_{i+1} (d_{NN} distance) (Billeter et al., 1982). Figure 1 summarizes the interresidue NOEs, along with the connectivities as defined by Zuiderweg et al. (1984). Also included in Figure 1 and Table II is the information about rapidly exchanging amide protons, and torsion angles derived from coupling constants, which together allow elements of secondary structure to be identified. These data identify the region Ala-14 to Cys-18 as a β-turn (Wüthrich et al., 1984), with Thr-16 and Gly-17 in the middle of the loop. Their amide protons are much more labile than those of Ala-14, Cys-15, and Cys-18.

The NOESY spectrum in H_2O suffers from problems of dynamic range owing to incomplete suppression of the solvent peak. We have therefore looked for interresidue NOEs in D_2O (Figure 7). The spin system of tyrosine was determined, as there are strong NOEs from the 2,6 protons of the ring to both the C^α and C^β protons. Because the α/β spin systems of tyrosine, asparagine, and cysteine are very similar, it is necessary to determine the tyrosine and asparagine spin systems separately. This assignment was further confirmed by using ST Ib(6–18), an analogue that lacks Tyr-19, in which the connectivity from the C^α proton at 5.2 ppm to the C^β protons at 2.9 ppm remains. The remaining connectivities can then be assigned to cysteines.

An important cross peak in the NOESY spectrum absent in the COSY spectrum connects the C^α proton of Asn-12 to one of the protons of Gly-17 (3.8 ppm). Irradiation of the Asn-12 C^α proton resonance (5.25 ppm; 25 °C) in the one-dimensional proton spectrum of ST Ib(6–19) gave measurable NOEs to one of the two Gly-17 C^α protons, confirming the result of the NOESY spectrum. The observation of this NOE cross peak (Figure 7) indicates that the turn Ala-14 to Cys-18 is folded over onto a structured region centered around Asn-12 and Pro-13, another possible β-turn segment (Chou & Fasman, 1974). A weaker NOE connectivity was also observed between the ring protons of Tyr-19 and the α-carbon proton of Asn-12. The C-terminal tyrosine ring is thus folded back onto the main structure.

(*6*) *Structure of the ST Peptide: Model Building and Verification.* Models of the structure of ST were derived in an iterative fashion by two programs (PROTO and NOEMOT) as follows. First, a CPK model of the C-terminal half of the molecule (Cys-10 to Tyr-19) was constructed, with the constraints that the distance between the α-carbon protons of Asn-12 and Gly-17 was smaller than 4 Å and the relative distances between α-carbon and amide protons would account for the $d_{\alpha N}$ and d_{NN} connectivities given in Figure 1. Figure 1. Only one basic conformation was possible, which did not allow a disulfide bond to connect Cys-15 and Cys-18. The N-terminal portion of the molecule was then added, and all possible combinations of disulfide bridges tried, except for the pairs Cys-15/Cys-18, Cys-6/Cys-7, or Cys-10/Cys-11. The last two combinations were eliminated because disulfide pairing involving adjacent cysteines have not been observed in proteins (Thornton, 1981) and in small cysteine-rich peptides such as conotoxins (Nishiuchi & Sakakibara, 1982; Gray et al., 1983, 1984), viscotoxin B (Samuelsson & Pettersson, 1971), crambin (Teeter et al., 1981), and ATX II (Wunderer, 1978; Wunderer & Eulitz, 1978). The structure of the C-terminus and the van der Waals constraints on the N-terminus provided sufficient constraints to suggest the pairing of Cys-6/Cys-15, Cys-7/Cys-11, and Cys-10/Cys-18 as a possible disulfide arrangement in agreement with the arrangement proposed by Houghten et al. (1984) on the basis of air-oxidation of the reduced peptide. All calculations were subsequently performed assuming this arrangement, although one cannot rule out other arrangements.

Starting with the peptide in a random coil configuration, the conformation was adjusted by the program PROTO until the best fit for the imposed constraints was obtained. Initially, these constraints were the van der Waals radii, ϕ angles determined from coupling constants, standard bond lengths and bond angles, distance ranges from NOE experiments, distance constraints on disulfide bridges, and the absence of hydrogen bonds for amide protons as determined from their exchangeability (section 2). Because NOE intensities contain contributions from a variety of pathways of magnetization transfer and are dependent on the actual geometry of the peptide, it is not possible to derive accurate distances from them; the observation of a NOE implies proximity of the protons to within 4 Å for a molecule of this size (Lane et al., 1986b). Because the structure is unknown a priori, the distance constraints from NOE measurements have to be liberal in the early stages of the structure determination. The coordinates obtained from a run of PROTO are then read into the program NOEMOT, which calculates the NOE time courses of all relevant protons. The relative intensities of the calculated NOEs are compared with the observed relative NOE intensities (for $d_{\alpha N}$, d_{NN}, and self $d_{\alpha N}$). The last intensities (self $d_{\alpha N}$) serve as internal controls, as the distance always lies in the range of 2.26–3.06 Å, and therefore should yield a NOE in the absence of other factors such as the rapid exchange of the amide protons. The comparison of the calculated and observed relative intensities shows which distance constraints are violated. For example, if the calculated NOE is vanishingly small and the observed NOE is large, then clearly the local structure is incorrect.

The new information serves as input for the program PROTO, and the procedure is repeated until all the constraints are satisfied. This cyclic process not only improves the agreement of the calculated and observed NOEs but also led to a reduction of van der Waals violations, owing to the improved interpretation of the experimental data as constraints. In later

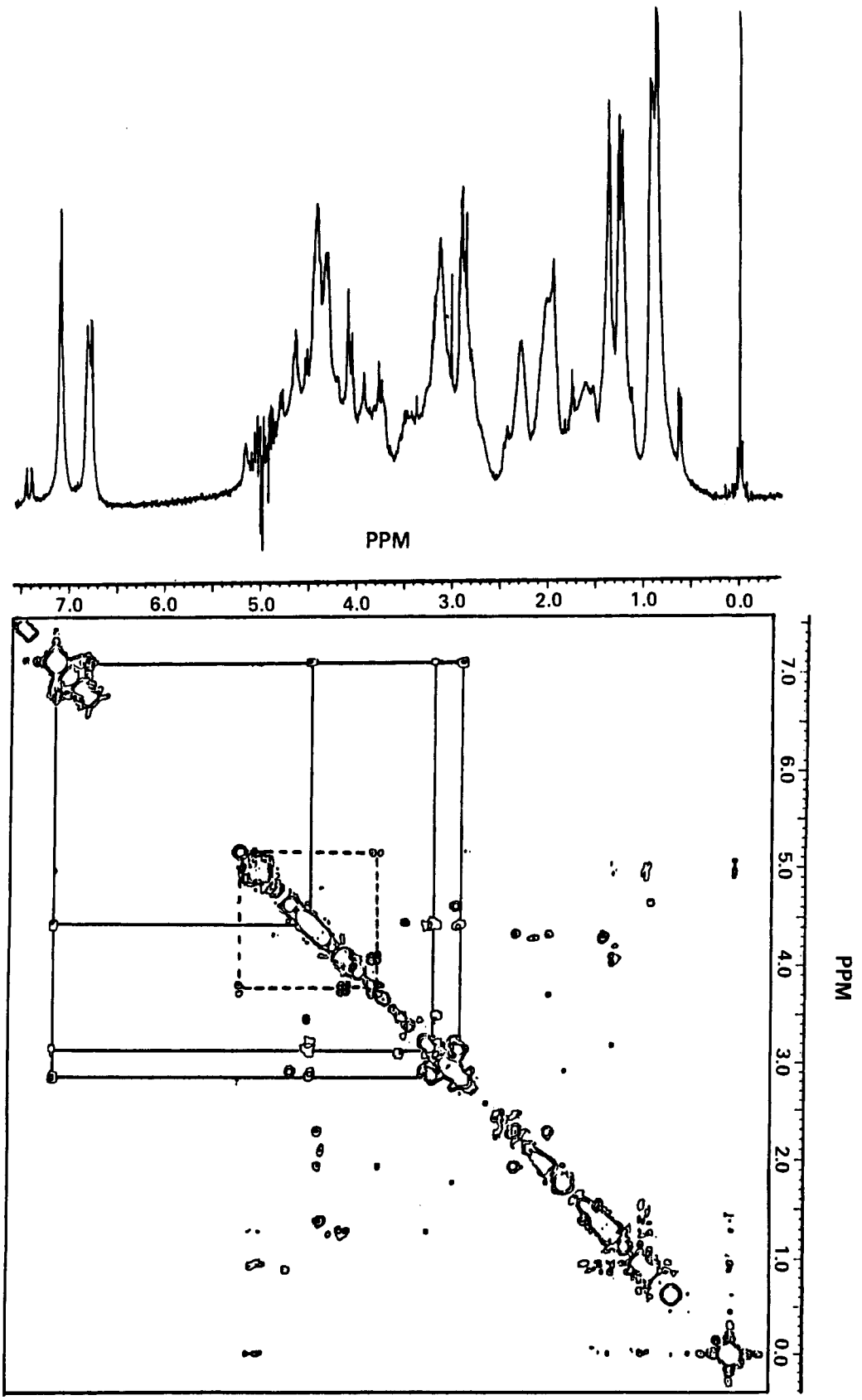

FIGURE 7: Contour plot of the region 0–7.5 ppm of the ^1H NOESY spectrum at 500 MHz of ST Ib(6–19) in D_2O. Conditions were as described in Figure 3. The mixing time was 500 ms. The solid lines retrace the spin system of Tyr-19, while the dotted lines highlight the NOE connectivity between Asn-12 (5.20 ppm) and Gly-17 (3.75 ppm) α-carbon protons.

stages of the refinement, the changes in the structure became smaller and localized to one or two backbone torsion angles. The derived set of coordinates yielded only one van der Waals violation where the β-carbon of Asn-12 and the α-carbon of Pro-13 are 2.77 Å apart (minimal distance expected is 3.2 Å). However, we know that the proline ring is not rigid and does not exist in a trans configuration at all times (section 3).

A stereo projection of the model is shown in Figure 8, along with a projection of the space-filling model. Table IV gives the values of the backbone torsion angles and, where appro-

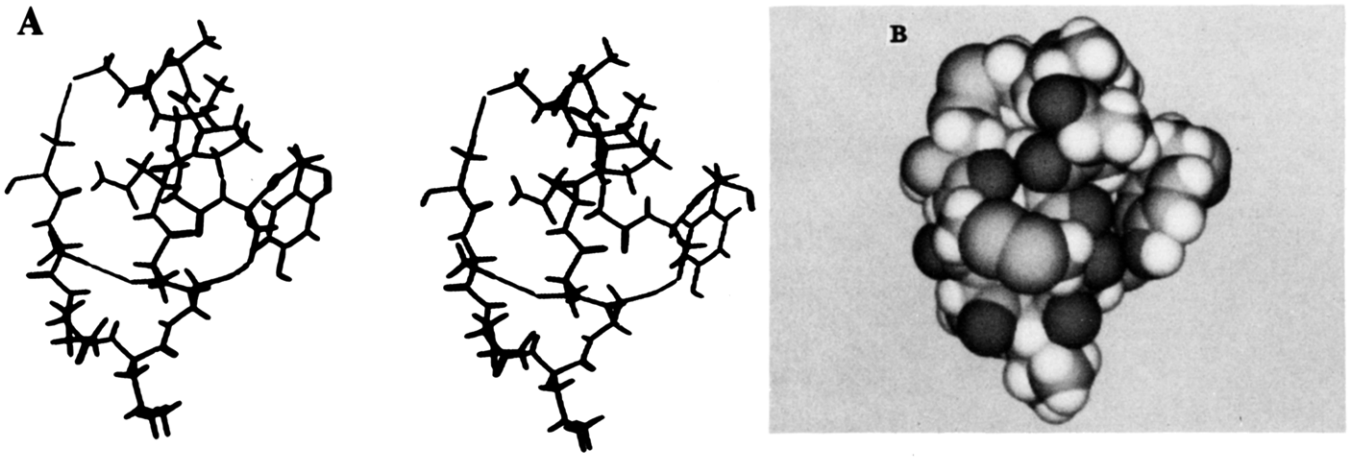

FIGURE 8: Proposed structure of ST Ib(6–19). A set of atomic coordinates was derived according to the text (section 6), and the resulting structure was displayed on an *Evans and Sutherland* graphics system using the program MOGLI. A stereo projection of the peptide and its equivalent space-filling representation illustrate the compactness of the molecule particularly in the C-terminal region.

Table IV: Comparison of Experimental and Calculated Relative NOE Intensities and Torsion Angles for C-Terminal Region of ST Ib(6–19)[a]

	structural parameters								
	exptl values				calcd values				
residue	$d_{\alpha N}^{self}$	$d_{\alpha N}$	d_{NN}	ϕ	$d_{\alpha N}^{self}$	$d_{\alpha N}$	d_{NN}	ϕ	ψ
Cys-10	0	0	m	nd	0	0	m	−60	−40
Cys-11	s	0	0	nd	s	s	0	65	202
Asn-12	0			60, −90, −150	w			−74	134
Pro-13		0		nd		0		−75	−52
Ala-14	w	w	s	25, 95, −85, −150	w	w	m	−133	48
Cys-15	s	s	0	nd	s	s	w	55	84
Thr-16	w	w	w	nd	w	0	m	−130	−70
Gly-17	w	0	m	nd	w	0	s	130	−180
Cys-18	w	s	m	60, −100, −140	w	s	w	−170	103
Tyr-19	m			60, −90, −150	m			−60	

[a] The torsion angles ϕ and ψ were calculated from the coordinates generated by the program PROTO (Frayman, 1985) and the experimental values were taken from Table II. The relative NOE intensities were calculated by the program NOEMOT described in the text (for τ_c = 1.6 ns at 10 °C). The experimental relative intensities were taken from NOESY spectra of ST Ib(6–19) recorded at 10 °C and were normalized to the cross peak connecting the 2,6 and 3,5 protons of Tyr-19. These intensities are reported for the observed interproton distances $d_{\alpha N}^{self}$, $d_{\alpha N}$, and d_{NN} (Figure 1, section 6). Nomenclature of intensities: s, strong; m, medium; w, weak; 0, not observed; nd, not determined.

priate, a comparison of the observed and calculated relative NOE intensities. The molecule is disc-shaped in agreement with our estimates of rotational correlation times (section 4). The C-terminal region is tightly packed, consisting of two successive turns (Cys-11 to Ala-14 and Cys-15 to Tyr-19). The N-terminal region is more loosely packed, reflecting the lack of available constraints as well as providing a possible explanation for the observed temperature-dependent change in the conformation of this region of the peptide.

During the preparation of this paper, an attempt has been made to propose a structure for ST Ib(6–19) in dimethyl sulfoxide based solely on a limited number of proton–proton distance constraints (Ohkubo et al., 1986) and a distance geometry algorithm (Braun & Gō, 1985). The C-terminal region in their model basically corresponds to ours (presence of two turns). However, the overall folding pattern of the peptide backbone differs significantly with the one proposed in our model since the ensemble of constraints used to generate their family of structures lacks any information concerning the disulfide linkages or the exchangeability of amide protons (i.e., non-hydrogen-bonded amide protons).

Our model is underdetermined for the following reasons. There are no sequential NOEs for the first four residues, so that their conformations are determined solely by the covalent structure, van der Waals radii, and the disulfide bonds. The arrangement of the disulfide bonds itself is tentative, though it does confirm to the proposal of Houghton et al. (1984). We also took no account of the cis–trans isomerization of the proline residue, the effect of which appears to be local. The model was built for the trans isomer. In the region from Cys-10 to Tyr-19, there are two long-range constraints on the conformation, namely, the disulfide link from Cys-10 to Cys-18 and the NOE between the C^{α} protons of Asn-12 and Gly-17. In addition, there are eight observed sequential NOEs in this region (out of a maximum of 15). Further, the absence of sequential NOEs for Cys-15 to Thr-16 and Thr-16 to Gly-17 (Table IV) allows lower limits to be placed on two distances. This is because the NOE between the $C^{\alpha}H$ to NH protons within a peptide unit (self $d_{\alpha N}$) provides an internal calibration. If self $d_{\alpha N}$ NOEs are observed for sequential residues such as Cys-15, Thr-16, and Gly-17, the absence of sequential $d_{\alpha N}$ NOEs cannot be ascribed to competing effects of exchange of the amide proton or to efficient relaxation, but rather to a long distance. The cross-relaxation rate constant for a molecule having a correlation time of 1.6 ns (in H_2O; 10 °C) is 0.12 s^{-1} for a distance of 3 Å and only 0.02 s^{-1} for a distance of 4 Å. Hence, unless there are other pathways of magnetization transfer, a NOE will not be observed, under our experimental conditions, at distances larger than 4 Å. Once the structure approaches self-consistency, the influence of alternative pathways of magnetization transfer can be calculated. These calculations indicated that the absence of NOEs for these protons implies a lower limit of 3.2 Å (calculated NOE <1%). Another possible difficulty of interpreting NOE in-

tensities in terms of distances is the problem of motional averaging. However, simulations that allowed movements of atoms up to 1 Å, and decreases in the correlation time by a factor of 2, indicated that the relative NOE intensities are not greatly affected, at least in the region of Cys-15 to Tyr-19. Because the number of constraints in the C-terminal region is relatively large, this portion of the molecule is quite well determined. The basic conformation of this region is independent of any assumptions about the exact arrangement of disulfide bonds. In contrast, the N-terminal region has a relatively greater freedom of movement, as evident from a lack of observable NMR constraints.

In summary, the model proposed in Figure 8 represents one conformation consistent with the set of disulfide linkages chosen and the constraints derived from the NMR results.

(*7*) *Sequence Homologies in Addition to Key Features of the Folded Structure Suggest the Importance of Gly-17 for Proper Folding of the Toxin.* The enterotoxic and receptor-binding properties of the toxin are coded by a 13-residue sequence (residues 6–18 of ST Ib). Ten of the 13 amino acid positions are conserved in ST I toxins isolated from enterotoxigenic *Escherichia coli* (Aimoto et al., 1982), *Vibrio cholerea* (Takao et al., 1985), and *Yersinia enterocolitica* (Takao et al., 1985) strains. Following the nomenclature of ST Ib used in this study (Aimoto et al., 1982; Moseley et al., 1983), all six cysteines are conserved (positions 6, 7, 10, 11, 15, 18) as well as Asn-12, Pro-13, Ala-14, and Gly-17. The substitutions of Glu-8 (*E. coli*) by aspartic acid (*Y. enterocolitica*) and Leu-9 by either isoleucine (*V. cholerea*) or valine (*Y. enterocolitica*) are conservative mutations involving a single codon base pair. The replacement of Thr-16 by either alanine (*E. coli*, ST Ia; *Y. enterocolita*) or phenylalanine (*V. cholerea*) suggests that this particular residue is not critical for folding or enterotoxicity. A consensus sequence would thus preserve all three disulfides as well as the two turns in the C-terminal region. Removal of the segment Gly-16 to Tyr-19 through chemical synthesis leads to a biologically inactive analogue (J. Gariépy and G. K. Schoolnik, unpublished results), implying the possible importance of the turn as well as a missing disulfide in the proper folding. The unique NOE between the α-carbon protons of Asn-12 and Gly-17 highlights the spatial proximity of these two regions of the peptide backbone. Since Asn-12 can be replaced by a tyrosine residue with only a partial loss of activity (Yoshimura et al., 1984), this particular side chain is not critical for either peptide folding or enterotoxicity. Note that this substitution may not have altered the possible turn in this region since tyrosine has itself a strong turn potential (Chou & Fasman, 1974) and the side chain at position 12 would be facing the solvent (Figure 8). However, the glycine residue is conserved in all ST I sequences (Takao et al., 1985), suggesting that a flexible residue having a small side chain may be required for the folding of the peptide chain at this position. We propose that the replacement of this residue by alanine or other amino acids should affect the folding and the activity of the new analogue.

In conclusion, we have prepared two active analogues of the *E. coli* heat-stable enterotoxin ST I and have analyzed their conformations in solution using nuclear magnetic resonance techniques. A model for the toxin's enterotoxic domain is proposed on the basis of geometric constraints derived from the NMR experiments and a pattern of disulfide linkages proposed by Houghten and his co-workers (Houghten et al., 1984). The C-terminal region from Cys-10 to Cys-18 is well-defined and provides a base for the design and analysis of new analogues. The N-terminal region cannot be defined from the available constraints, and this may reflect its greater mobility.

ACKNOWLEDGMENTS

We are grateful to Drs. K. Faull, O. Beck, and D. Jones for running mass spectra on the peptide and to Drs. J.-F. Lefèvre and T.W.-M. Fan for fruitful discussions of the problem.

Registry No. ST Ib(6–19), 104740-75-2; ST Ib(6–18), 104740-76-3.

REFERENCES

Aimoto, S., Takao, T., Shimonishi, S., Hara, T., Takeda, T., Takeda, Y., & Miwatani, T. (1982) *Eur. J. Biochem. 129*, 257–266.

Arseniev, A. S., Kondakov, V. I., Maiorov, V. N., & Bystrov, V. F. (1984) *FEBS Lett. 165*, 57–62.

Bax, A. (1981) Ph.D. Thesis, University of Groningen, The Netherlands.

Billeter, M., Braun, W., & Wüthrich, K. (1982) *J. Mol. Biol. 155*, 321–346.

Booth, B. R., Wolffe, E. J., & Sowa, M. A. (1984) *Biochem. Soc. Trans. 12*, 268–269.

Bothner-By, A. A., & Noggle, J. H. (1979) *J. Am. Chem. Soc. 101*, 5152–5160.

Braun, W., & Gō, N. (1985) *J. Mol. Biol. 186*, 611–626.

Bystrov, V. F. (1976) *Prog. Nucl. Magn. Reson. Spectrosc. 10*, 41–81.

Cantor, C. R., & Schimmel, P. R. (1981) in *Biophysical Chemistry*, Part II, pp 552 and 655, W. H. Freeman, San Francisco.

Cung, M. T., Marraud, M., & Neel, J. (1974) *Macromolecules 7*, 606–613.

De Marco, A., Llinas, M., & Wüthrich, K. (1978) *Biopolymers 17*, 637–650.

Dreyfus, L. A., & Robertson, D. C. (1984) *Infect. Immun. 46*, 537–543.

Englander, S. W., & Kallenbach, N. R. (1984) *Q. Rev. Biophys. 16*, 521–653.

Field, M., Graf, L. H., Jr., Laird, W. J., & Smith, P. L. (1978) *Proc. Natl. Acad. Sci. U.S.A. 75*, 2800–2804.

Frantz, J. C., Jaso-Friedmann, L., & Robertson, D. C. (1984) *Infect. Immun. 43*, 622–630.

Frayman, F. (1985) Ph.D. Thesis, Northwestern University, Evanston, IL.

Gariépy, J., & Schoolnik, G. K. (1986) *Proc. Natl. Acad. Sci. U.S.A. 83*, 483–487.

Gariépy, J., O'Hanley, P., Waldman, S. A., Murad, F., & Schoolnik, G. K. (1984) *J. Exp. Med. 160*, 1253–1258.

Giannella, R. A., & Drake, K. W. (1979) *Infect. Immun. 24*, 19–23.

Giannella, R. A., Luttrell, M., & Thompson, M. (1983) *Am. J. Physiol. 245*, G492–G498.

Gooley, P. R., & Norton, R. S. (1985) *Eur. J. Biochem. 153*, 529–539.

Gooley, P. R., Beress, L., & Norton, R. S. (1984a) *Biochemistry 23*, 2144–2152.

Gooley, P. R., Blunt, J. W., & Norton, R. S. (1984b) *FEBS Lett. 174*, 15–19.

Gray, W. R., Luque, A., Olivera, B. M., Barrett, J., & Cruz, L. J. (1981) *J. Biol. Chem. 256*, 4734–4740.

Gray, W. R., Rivier, J. E., Galyean, R., Cruz, L. J., & Olivera, B. M. (1983) *J. Biol. Chem. 258*, 12247–12251.

Gray, W. R., Luque, F. A., Galyean, R., Atherton, E., Sheppard, R. C., Stone, B. L., Reyes, A., Alford, J., McIntosh, M., Olivera, B. M., Cruz, L. J., & Rivier, J.

(1984) *Biochemistry 23*, 2796–2802.
Gupta, R. J., Ferretti, J. A., Becker, E. D., & Weiss, G. H. (1980) *J. Magn. Reson. 38*, 47–52.
Hore, P. J. (1983) *J. Magn. Reson. 55*, 283–300.
Houghten, R. A., Ostresh, J. M., & Klipstein, F. A. (1984) *Eur. J. Biochem. 145*, 157–162.
Hughes, J. M., Murad, F., Chang, B., & Guerrant, R. L. (1978) *Nature (London) 271*, 755–756.
Kearns, D. R. (1984) *CRC Crit. Rev. Biochem. 15*, 237–286.
Kuno, T., Kamisaki, Y., Waldman, S. A., Gariépy, J., Schoolnik, G. K., & Murad, F. (1986) *J. Biol. Chem. 261*, 1470–1476.
Lane, A. N., Lefèvre, J.-F., & Jardetzky, O. (1986a) *Biochim. Biophys. Acta 867*, 45–56.
Lane, A. N., Lefèvre, J.-F., & Jardetzky, O. (1986b) *J. Magn. Reson. 66*, 201–218.
Lefèvre, J.-F., Lane, A. N., & Jardetzky, O. (1985) *J. Mol. Biol. 185*, 689–699.
Molday, R. S., Englander, S. W., & Kallen, R. G. (1972) *Biochemistry 11*, 150–159.
Moseley, S. L., Hardy, J. W., Imdadul Huq, M., Echeverria, P., & Falkow, S. (1983) *Infect. Immun. 39*, 1167–1174.
Nagayama, K. (1981) *Adv. Biophysics 14*, 139–204.
Nishiuchi, Y., & Sakakibara, S. (1982) *FEBS Lett. 148*, 260–262.
Ohkubo, T., Kobayashi, Y., Shimonishi, Y., Kyogoku, Y., Braun, W., & Gō, N. (1986) *Biopolymers* (in press).
Olejnicjak, E. T., Poulsen, F. M., & Dobson, C. M. (1984) *J. Magn. Reson. 59*, 518–523.
Ramachandran, G. N., Chandrasekaran, R., & Kopple, K. D. (1971) *Biopolymers 10*, 2113–2131.
Richardson, J. S. (1981) *Adv. Protein Chem. 34*, 168–339.
Sack, R. B. (1980) *J. Infect. Dis. 142*, 279–286.
Samuelsson, G., & Pettersson, B. M. (1971) *Acta Chem. Scand. 25*, 2048–2054.
So, M., & McCarthy, B. J. (1980) *Proc. Natl. Acad. Sci. U.S.A. 77*, 4011–4015.
Takao, T., Tominaga, N., & Shimonishi, Y. (1984) *Biochem. Biophys. Res. Commun. 125*, 845–851.
Takao, T., Shimonishi, Y., Kobayashi, M., Nishimura, O., Arita, M., Takeda, T., Honda, T., & Miwatani, T. (1985) *FEBS Lett. 193*, 250–254.
Teeter, M. M., Mazer, J. A., & L'Italien, J. J. (1981) *Biochemistry 20*, 5437–5443.
Thompson, M. R., & Giannella, R. A. (1985) *Infect. Immun. 47*, 834–836.
Thornton, J. M. (1981) *J. Mol. Biol. 151*, 261–287.
Wagner, G. (1983) *Q. Rev. Biophys. 16*, 1–57.
Wagner, G., & Wüthrich, K. (1979) *J. Magn. Reson. 33*, 675–680.
Walsh, J. A., & Warren, K. S. (1979) *N. Engl. J. Med. 301*, 967–974.
Williamson, M. P., Marion, D., & Wüthrich, K. (1984) *J. Mol. Biol. 173*, 341–359.
Wunderer, G. (1978) *Hoppe-Seyler's Z. Physiol. Chem. 359*, 1193–1201.
Wunderer, G., & Eulitz, M. (1978) *Eur. J. Biochem. 89*, 11–17.
Wüthrich, K. (1976) in *NMR in Biological Research: Peptides and Proteins*, Chapter V, North-Holland, Amsterdam.
Yoshimura, S., Miki, M., Ikemura, H., Aimoto, S., Shimonishi, Y., Takeda, T., Takeda, Y., & Miwatani, T. (1984) *Bull. Chem. Soc. Jpn. 57*, 125–133.
Yoshimura, S., Ikemura, H., Wanatabe, H., Aimoto, S., Shimonishi, Y., Saburo, H., Takeda, T., Miwatani, T., & Takeda, Y. (1985) *FEBS Lett. 181*, 138–142.
Zamyatnin, A. A. (1984) *Annu. Rev. Biophys. Bioeng. 13*, 145–165.
Zuiderweg, E. R. P., Kaptein, R., & Wüthrich, K. (1983) *Proc. Natl. Acad. Sci. U.S.A. 80*, 5837–5841.